This is a preprint, the final version is subject to change, of the American Mineralogist (MSA)
Cite as Authors (Year) Title. American Mineralogist, in press.
DOI: https://doi.org/10.2138/am-2020-7227

Revision 2

Characterization of modified mineral waste material adsorbent as affected by thermal treatment for optimizing its adsorption of lead and methyl orange

Su, Lingcheng[1], Chen, Jiajun.[1], Ruan, Huada.[1*], Chen, Dongqi.[1], Chen, Xi.[1], and Lee, Chiuhong. [1]

[1]Environmental Science Program, Division of Science and Technology, Beijing Normal University-Hong Kong Baptist University United International College, No. 2000 Jingtong Road, Zhuhai, China, 519082. [*]Corresponding author (*Email address:* hruan@uic.edu.hk)

Abstract

Thermal treatment is one of the most common processes in mineral modification and this process has been applied to the modification of mineral waste material to improve its adsorption ability of methyl orange (MO) and lead (Pb) in this study. The properties of modified mineral waste material (MMWM) before and after thermal modification were characterized by using the Brunauer–Emmett–Teller (BET) N_2 adsorption/desorption measurement, field emission scanning electron microscope (FESEM) coupled with energy dispersive X-ray (EDX), X-ray diffraction (XRD) and Fourier transform infrared spectroscopy (FTIR). Phase transformation related to the change in surface morphology and dehydroxylation that occurred in MMWM samples during the process of thermal treatment were investigated. To study adsorption performances of Pb and MO onto the newly modified MMWM, a number of experiments were carried out under different adsorption conditions and the results were determined using inductively coupled plasma optical emission spectrometry

(ICP-OES) and UV-Vis spectrophotometry. The thermally treated MMWM samples showed morphological transformation, and an increasing trend in BET specific surface area (SSA) up to 500 ℃ followed by a decreasing trend till 1000 ℃. Thermal modification of MMWM had successfully improved Pb adsorption from 349 to 515 mg/g, corresponding to the MMWM modified at 600 ℃, and the methyl orange (MO) adsorption from 68 to 87.6 mg/g at 400 ℃. The adsorptions of Pb and MO were mainly chemisorption and monolayer coverage, as the pseudo-second-order model and the Langmuir equation displayed good correlations for Pb and MO adsorption data.

Keywords: Adsorption, dehydroxylation, lead (Pb), methyl orange (MO), modified mineral waste material (MMWM)

Introduction

The modified mineral waste material (MMWM) is a mixed clay mineral type of adsorbent that was originally derived from industrial mineral waste after physical and chemical modifications (Jiang et al. 2013a). It can be used as a low-cost, environmentally safe adsorbent and found to have strong adsorption abilities (Jiang et al. 2013b). Consisting primarily of smectite and illite, MMWM shows great ability in adsorbing pollutants from water, soil and air which have been applied in our previous experiments for removing environmental pollutants (Jiang et al. 2014; Lu et al. 2016). These investigations have confirmed that the MMWM has better adsorption abilities

of heavy metals (lead (Pb), copper (Cu) and cadmium (Cd)) in solution than activated carbon (AC) (Lu et al. 2016). MMWM was also found to have the ability to adsorb organic compounds from wastewater such as organic phosphate (Jiang et al. 2014). The adsorptive efficiency of some organic pollutants is found to be even better than AC.

As one of the main components in MMWM, the smectite group of clays (e.g. montmorillonite) is normally abundant and has extraordinary properties which make it a compelling and reasonable precedent for a low cost and effective adsorbent (Rathnayake et al. 2017). Smectite is comprised of a number of clay minerals consisting of tetrahedral-octahedral-tetrahedral (t-o-t) layers of both dioctahedral and trioctahedral types (Hurlbut and Klein 1977; Bhattacharyya and Gupta 2008). Similar to smectite (e.g. montmorillonite), illite is another kind of clay mineral in MMWM. It can be defined as the mineral occurring in the clay fraction with Al–K, is non-expanding, di-octahedral with mica-type properties, and is a mineral that is commonly used in the traditional ceramic industry and can be applied in the removal of heavy metals in solution (Srodon and Eberl 1984; Ozdes et al. 2011; Csáki et al. 2017; Húlan et al. 2017). On the other hand, the swelling properties of the 2:1-layer silicates (e.g. montmorillonite) result in an increased water and contaminants retention ability, which is dependent on the interlayer spacing upon the charge of layer, hydration energy, chemical potential and relative humidity (Tambach et al. 2004; Fonseca et al. 2017).

Investigations pertaining to the use of mineral related adsorbents have a long history, and the high adsorption capabilities of clay minerals are the result of the net negative charges on the lattice of minerals. These negative charges will be neutralized by the adsorption of positively charged contaminants, providing clay adsorbents the ability to attract and hold cations such as heavy metals (Bailey et al. 1999). The maximum adsorption capacity of Pb for natural goethite is observed to be 109.2 mg/g (Lounis et al. 2012). The maximum adsorption capacities of kaolinite (Cd 11.4 mg/g, Cr (VI) 13.9 mg/g, Pb 82.65 mg/g) and montmorillonite (Cd 33.2 mg/g, Pb 31.3 mg/g) are achieved after activation of these minerals (Alvarez-ayuso and Garcia-Sanchez 2003; Adebowale et al. 2008; Sen and Bhattacharyya 2008). Ozdes et al. (2011) reported that the maximum adsorption capacity of illite towards Pb (239 mg/g) can be achieved when the adsorption is conducted at pH = 4 and room temperature for 240 mins. A group of modified mineral adsorbents has been used in removing Pb from aqueous solution and the adsorption capacities of the clays for Pb are 22.7 mg/g and 6.3 mg/g for acid-activated montmorillonite and kaolinite respectively (Bhattacharyya and Gupta 2008). Bhatnagar et al. (2006) reported that the adsorption of Pb on adsorbents prepared from industrial wastes (blast furnace sludge) is as high as 227 mg/g. The maximum adsorption capacity of beidellite for Pb is 86.9 mg/g, and the polymer/montmorillonite clay nanocomposite, imprinted by zinc ion, can adsorb a maximum of 301 mg/g Pb (Etci et al. 2010; Msaadi et al. 2017). The adsorption of Pb on rectorite is mainly dominated by surface complexation and cation exchange, with

the equilibrium adsorption capacity being 17.9 mg/g (Msaadi et al. 2017). Beside metal pollutants, mineral adsorbents are also applied for removal of organic contaminants such as dyes. Methyl orange (MO) is a kind of anionic dye that has been widely applied in the printing industry, but it is unfortunately toxic and carcinogenic (Eljiedi et al. 2017). One new material, uncalcined glycerol-modified nanocrystallined Mg/Al layered double hydroxides, is applied as a good adsorbent for MO removal (Yao et al. 2017). Habiba et al. (2017) suggested that the removal of MO in wastewater could be predominated by adsorption at low initial concentrations, whereas flocculation was observed at high concentrations.

A number of methods have been developed for the modification of clay mineral adsorbents. Mechanochemical activation such as the grinding treatment is used for kaolinite modification. The process can be identified as the creation of a new amorphous material with the destruction of kaolinite, and then an agglomerated material is produced by the aggregation of the ground particles (Kelley 1957; Takahashi 1959; Frost et al. 2004). Dehydroxylation, which results in the release of physically and chemically bounded water, is one of the most significant phenomena occurring during thermal treatment of clay mineral. By investigating the kinetic of dehydroxylation in clay mineral, the dehydroxylation concept of kaolinite can be expressed as a result of the interaction between two hydroxyl groups to form a water molecule by proton transfer, leaving chemically bonded oxygens (oxide anion) in the

lattice (Miller and Oulton 1970). The reactions are shown as the following (Frost et al. 2004):

$$-OH^- \Leftrightarrow H^+ + -O^{2-}$$

$$H^+ + -OH^- \Leftrightarrow -H_2O$$

The hysteresis occurred during the hydroxylation and dehydroxylation processes of intercalated cations. Some studies conclude that the transition from two- to one-layer hydroxylated montmorillonite is harder than that from one water layer to completely dehydroxylate, which is joined by a diminishing of the basal spacing and a change in the contrary ion and the water atoms, other than the arrangement of hydrogen bonds being obviously weak (Fonseca et al. 2017). The transition of montmorillonite is temperature dependent. Dehydroxylation and desorption of physically adsorbed water molecules occur between 30 and 150 °C, decomposition of ammonium cations and dehydroxylation of structural water between 400 and 600 °C, and transformation of intercalated hydroxylated species to metal oxides at above 750 °C (Ruan and Gilkes 1996; Elkhalifah et al. 2013; Martinez et al. 2017). GuccnNnnrtr et al. (1978) reported that the dehydroxylation of dioctahedral 2:1-layer silicates (e.g. muscovite) is not a homogeneous process, the strength of the Al-OH bond can be greatly affected by the coordination number of neighbouring polyhedra. This can be classified by using a muscovite dehydroxylation model, the loss of hydroxyl groups of neighbouring polyhedra in octahedral coordination occurs more than five-fold at lower temperatures, which results in the distribution of oversaturated apical oxygens that also affect the

126 proton position and the Al-OH bond strength (GuccnNnnrtr et al. 1978). For
127 dehydroxylation of illite at temperature intervals from 450 to 700 °C, the initial step
128 can be comprised of the condensation of OH- groups inside the octahedral layer and a
129 resulting 1-D dispersion of the simply framed water atoms through tetrahedral rings
130 into an interlayer region; and the second step can be represented by a 2-D dispersion
131 of water particles far from the interlayer space (Csáki et al. 2017; Húlan et al. 2017).

132 The aims of this research are to figure out the most suitable conditions for thermal
133 modification of MMWM to improve its adsorption ability, and the characterization of
134 physicochemical and mineralogical properties of MMWM before and after thermal
135 treatment in relation to the dehydroxylation process and phase transformation; and to
136 investigate the abilities and kinetics of adsorptions of Pb and MO, which are the
137 representatives of metals and organic compounds, onto this newly modified MMWM.

138 Experimental and analytical methods

139 Mineral waste material collection and modification

140 The modified mineral waste material (MMWM) was obtained from a commercial
141 company in Hong Kong after an initial physical and chemical treatment (Jiang et al.
142 2013a; Lu et al. 2016). The sample was ground with an agate mortar and sieved to
143 0.015 mm, packaged in air-tight polyethylene (PE) bags and reserved in a vacuumed
144 desiccator.

For thermal treatment, MMWM sub-samples were heated at temperatures from 300 to 1000 ℃ with a 100 ℃ increment between samples for 120 mins in a vacuumed tube oven. To prevent reintroducing moisture, once the samples were cooled down to 200 ℃ inside the oven they were immediately transferred into a desiccator for further cooling down to room temperature. These samples were kept in polyethylene (PE) bags and reserved in a vacuumed desiccator before analysis. The un-heated MMWM sample was labelled as "MM un-heated" and the heated MMWM samples were labelled as MM 300, MM 400, etc., where the MM denoted MMWM and the number denoted the thermal treatment temperature.

Analysis of chemical composition of MMWM

A homogenized sample (approximately 200 mg) was first mixed with 10 ml of strong acid (4:1 concentrated 65% HNO_3 and 40% HF (v/v)) in an airtight Teflon tank (effective volume 50 mL) and was then heated at 180 ℃ in the microwave digester (Sineo, MDS-10, Shanghai, China) for 20 mins. After cooling down to room temperature, the supernatant was separated from the solid particles by vacuum filtration through a 0.22 μm filter and diluted to 100 mL with deionized (DI) water. The concentrations of metals (calcium (Ca), iron (Fe), aluminum (Al), magnesium (Mg), titanium (Ti), manganese (Mn), strontium (Sr), zinc (Zn), rubidium (Rb), barium (Ba), copper (Cu), etc.) in the digested solutions were determined using

164 inductively coupled plasma optical emission spectrometry (ICP-OES, Perkin-Elmer
165 Optima 2100 DV, USA).

166 **Investigation of the properties of MMWM**

167 ***Burnauer, Emmett, and Teller (BET) specific surface area***

168 The specific surface area (SSA) of MMWM was determined by the BET method
169 (thirteen-point liner plot) using nitrogen adsorption. Prior to measurements, samples
170 were outgassed at 120 ℃ for 12 hrs. The SSA was detected and calculated by using
171 Beckman Coulter, SA3100 surface area analyzer; the adsorption isotherms achieved a
172 p/p_0 range of 0.009-0.25.

173 ***Fourier transform infrared (FTIR) spectroscopy***

174 Fourier transform infrared absorption spectra of samples were obtained by using a
175 PerkinElmer Frontier FT-IR/NIR spectrometer. The MMWM samples were dispersed
176 in potassium bromide (KBr) with a KBr:MMWM ratio of 100:1. The mixtures were
177 ground to fine powder and pressed into lamellar forms to make disks. A wavenumber
178 range between 4000 and 450 cm^{-1} was recorded at a resolution of 4.0 cm^{-1} and 32
179 scans. The spectral manipulation including baseline adjustment, smoothing and
180 normalization was performed using Origin Pro 2017 (OrginLab Corporation,
181 Northampton, MA 01060 USA)

Field emission scanning electron microscopy (FESEM)

A representative portion of MMWM sample was sprinkled onto a double-sided carbon tape mounted on a SEM stub. All the samples were sprayed with a coat of gold before analysis. The FESEM measurements were performed on a high-resolution LEO 1530 field emission scanning electron microscope coupled with an energy dispersive X-ray detector from OXFORD.

X-ray diffraction (XRD) analysis

Sub-samples of un-heated and heated MMWM were prepared for XRD by grinding 500 mg of each sample and back filling in a quartz plate holder. Analysis was conducted via XRD by using non-monochromatic Cu $K\alpha$ radiation on a computer-controlled Bruker AXS D8 advanced X-Ray diffractometer. The step time of scans was 53.1 s and the step size was 0.02 ° 2θ. Patterns were recorded from 10 to 75 ° 2θ.

Adsorption experiments

Methyl orange adsorption

Batch experiments were carried out to determine the adsorption ability of MMWM towards MO. An initial experiment was conducted to determine the maximum adsorbent dosage of MO per unit of MMWM. For this purpose, 0.01, 0.02, 0.03, 0.04 and 0.05 g of adsorbents were dispersed in 50 ml of 100 mg/L MO solutions. The mixture in the flask was agitated on a shaker at room temperature (25 °C) for 480, 540,

600, 660 and 720 mins and filtered with a 0.22 μm filter. The solution was analyzed using a UV-Vis spectrophotometer (Thermo, Evolution 220, USA) coupled with an auto sampler with the detector being operated at 465 nm.

After the initial experiment, the adsorption capacity of MMWM was calculated, and the MMWM with the highest MO adsorption ability (0.04 g) was selected and categorized according to the design of intercalation method and kinetic and isothermal experiments. Adsorption kinetic experiment performed at room temperature (25 °C) and at pH = 7 was conducted by dispersing 0.04 g of the adsorbent in 50 ml of 100 mg/L MO solution in a flask. The amount of adsorbent selected was based on approximately 80% of MO being removed from solution at the equilibrium point. Then all the flasks were capped and placed in a shaker bath maintained at 25 °C and shaken at a speed of 300 rpm. The samples after MO adsorption were collected at different time intervals (1, 2, 3, 5, 15, 20, 30, 60, 120, 180, 240, 300, 360, 420, 480 and 540 mins) and filtered with a 0.22 μm filter to collect the supernatants. Adsorption isotherm studies were carried out by placing 0.04 g of MMWM in various volumes (15, 20, 25, 30, 35, 40, 45, and 50 mL) of 100 mg/L MO solutions under the same temperature and shaking speed as for the kinetic experiment. The samples after MO adsorption were collected at 540 mins and filtered with a 0.22 μm filter to collect the supernatants. The collected supernatants of both kinetic and isotherm experiments were analyzed using a UV-Vis spectrophotometer (Thermo, Evolution 220, USA) coupled with an auto sampler with the detector being operated at 465 nm.

Lead adsorption

Similar to the MO adsorption, an initial experiment of Pb adsorption was undertaken to find out the optimal adsorbent dosage of Pb per unit of MMWM. For this purpose, 0.01, 0.02, 0.03, 0.04 and 0.05 g of adsorbents were dispersed in 50 ml of 350 mg/L Pb solutions. The mixture in the flask was agitated on a shaker with a shaking speed of 300 rpm for 840 mins at room temperature (25 °C), and then filtered with a 0.22 μm filter. The solution after filtration was analyzed using ICP-OES (Perkin Elmer Optima 2100DV, USA).

After the initial experiment, the MMWM with the highest Pb adsorption ability (0.02 g) was selected and categorized according to the design of intercalation method and kinetic and isothermal experiments. Adsorption kinetic experiment performed at room temperature (25 °C) and at pH = 7 was conducted by dispersing 0.02 g of the selected adsorbent in 50 ml of 350 mg /L Pb solution. Then all the flasks were capped and placed in a shaker bath with the temperature set at 25 °C and shaken at a speed of 300 rpm. The samples after Pb adsorption were collected at different time intervals (5, 10, 20, 30, 60, 120, 180, 240, 300, 360, 420, 480, 560 and 840 mins) and filtered with a 0.22 μm filter to collect the supernatants. Adsorption isotherm studies were carried out by placing 0.02 g of MMWM in various volumes (5, 10, 15, 20, 25, 30, 35, 40, 45, and 50 mL) of 350 mg/L Pb solutions. The mixture in the flask was agitated on a shaker with a shaking speed of 300 rmp for 840 mins at room temperature (25 °C). The samples after Pb adsorption were collected at 840 mins and filtered with a 0.22

243 μm filter to collect the supernatants. The Pb concentrations in the collected
244 supernatants of both kinetic and isotherm experiments were determined using ICP-
245 OES.

246 ***Analysis of adsorption kinetics***

247 The amount of Pb and MO adsorbed onto the sample at different periods (*qt*) can
248 be calculated by the equation (1);

249 $$q_t = \frac{(C_0 - C_t) \times V_0}{m} \quad (1)$$

250 where C_0 and C_t are the concentrations of Pb or MO at initial and different time
251 intervals (mg/L), respectively; V_0 is the volume of Pb or MO solution (L) added, and
252 *m* is the amount of adsorbent (g) added.

253 To model the kinetic of Pb and MO adsorptions, the adsorption data were fitted to
254 the pseudo-second-order model, which can be described using equations (2) and (3)
255 (Frost et al. 2004)

256 $$\frac{t}{q} = \frac{1}{k{q_e}^2} + \frac{1}{q_e} t \quad (2)$$

257 which can be rewritten as:

258 $$q = \frac{k{q_e}^2 t}{1 + k q_e t} \quad (3)$$

259 Where q_e and q are the amounts of Pb or MO adsorbed by adsorbent at initial and
260 different time *t* (min) intervals (mg/g), respectively; *k* is the adsorption rate constant
261 of the pseudo-second-order model.

For the isotherm study, the equilibrium adsorption capacity (q_e) can be calculated by the equation (4);

$$q_e = \frac{(C_0 - C_e) \times V_0}{m} \quad (4)$$

Where C_0 and C_e are the initial and equilibrium Pb or MO concentration in solution (mg/L); V_0 is the volume of Pb or MO solution (L) added and m is the mass of adsorbent (g) added.

The Langmuir equation models the monolayer adsorption on the adsorbent surface (Langmuir 1917). Freundlich equation is based on the assumption that the adsorbent has a heterogeneous surface composed of different adsorption sites (Freundlich 1907). The equilibrium data were fitted to the Langmuir and Freundlich isotherm models shown in equations (5) and (6), respectively.

$$\text{Langmuir equation: } q_e = q_m K_l \frac{C_e}{1 + K_l C_e} \quad (5)$$

$$\text{Freundlich equation: } q_e = K_f C_e^{\frac{1}{n}} \quad (6)$$

where C_e (mg/L) is the Pb or MO concentration of solution at equilibrium point, q_e (mg/g) is the adsorption capacity of adsorbent at equilibrium point, q_m (mg/g) is the maximum adsorption capacity and K_l is the Langmuir adsorption equilibrium constant related to adsorption capacity and energy or net enthalpy of adsorption. K_f and n are the constants in the Freundlich isotherm model, which measure the adsorption capacity and intensity, respectively.

Results and discussion

Chemical composition of MMWM

The metal concentrations of MMWM determined by ICP-OES after microwave assisted digestion are shown in Table 1. Calcium, Fe, Al and Mg were the four most abundant metals. As expected, these four important metals in MMWM were present in over 98.7% of the total metal content. These results are similar to that of Jiang et al. (2013a), who reported that calcium silicate hydrate ($Ca_6Si_6O_{17}(OH)_{17}$) and calcium aluminum silicate hydrate ($CaAl_2Si_2O_8 \bullet H_2O$) were the two most abundant chemical compounds in MMWM, and Ca, Fe, Al and Mg were also the major metal compositions of montmorillonite, illite and chlorite. Krupskaya (2017) characterized the chemical composition of acid modified montmorillonite and found that Ca, Mg, Fe, and Al were the four most abundant metals. Aluminum is the main constituent of the octahedral layer $[AlO_3(OH)_3]^{6-}$, and Ca, Mg are the compositions of the exchangeable interlayer. The remaining metals, such as Ti, Mn, Sr, Zn, Rb, Ba and Cu that were detected at very low or trace concentrations, were present in less than 1.2% of the total metal content.

297 **Change in property after thermal modification**

298 ***Change in Burnauer, Emmett, and Teller (BET) specific surface area (SSA)***

299 To investigate the variation of SSA of MMWM as affected by thermal treatment,
300 N_2-adsorption /desorption was carried out for each sample. Figure 1 demonstrates the
301 variation of SSA of MMWM before and after thermal treatment at different
302 temperatures. The appearance of thermally treated MMWM samples that were
303 changing corresponded to the variations in temperature. The color of samples turned
304 from white grey into pink grey and more obvious changes in color was observed at
305 higher temperatures. It was clearly demonstrated that the SSA of thermally treated
306 samples increased from 4.070 to 6.496 m^2/g when the temperature was increased to
307 500 ℃ (Fig. 1). This could be attributed to the loss of water molecules and the change
308 in mineral layer structures, e.g. amorphous and/or meta-phases formed during thermal
309 transformation of minerals (Ruan and Gilkes 1996; Martinez et al. 2017). The SSA
310 then decreased to 0.874 m^2/g after heating to 1000 ℃, where the reformation of
311 crystal structures occurred. The MMWM samples used in this study consisted mainly
312 of clay minerals. Hydroxylation and dehydroxylation may occur easily in these typical
313 mineral structures, particularly on the surface structures. It is expected that the
314 changes in mineral surface structure can greatly enhance its adsorption ability.
315 Although the SSA of MMWM was much smaller than that of a typical activated
316 carbon (AC), the adsorption of metal pollutants per unit amount was always much
317 higher than that of AC (Lu et al. 2016). This study suggests that the greater adsorption

318 ability of MMWM could be contributed by the hydroxyls on the mineral surface. The
319 chemical bonding of adsorption formed by the release of loosely bonded water
320 molecules and the enlargement of surface area during thermal treatment at 500 °C and
321 lower temperatures also contributed to elevate the absorption ability of MMWM. It is
322 believed that such changes in structure, including the creation of defects in mineral
323 surface, may provide more adsorption sites and further increase its affinity for
324 adsorption (Ruan and Gilkes 1996).

325 ***Fourier transform infrared (FTIR) analysis for chemical bonding***

326 Infrared spectra are plotted to characterize the surface properties of MMWM, the
327 changes in bonded water molecules on the surface, and in the interlayer and mineral
328 structure during thermal modification. The infrared spectra of MMWM in the
329 vibrational range of 4000-450 cm^{-1} are displayed in Fig. 2. The changes in infrared
330 spectra are obviously observed from MM un-heated to MM 1000. The disappearance
331 of a band at 1639 cm^{-1} first occurs in the spectrum of MM 300, and the intensity of
332 the band at 1428-1415 cm^{-1} decreases with increasing temperatures (MM 300, MM
333 400, MM 500, MM 600, and MM 700 of Fig. 2) and completely disappears in the
334 spectrum of MM 700. Another broad band can be observed at 3448-3442 cm^{-1} from
335 the spectra of MM un-heated and MM 300, but it disappears when the thermal
336 treatment temperature reaches higher than 400 °C. This can be attributed to the release
337 of absorbed or loosely bonded surface water. One intense water bending band at 1639

338 cm^{-1} and three intense hydroxyl deformation bands at 875-726 cm^{-1} are observed and
339 assigned to different OH modes. Two fundamental vibrational modes of adsorbed
340 water molecules on MMWM are observed in FTIR spectra: a group of symmetric O-
341 H stretching vibrations in the spectral regions of 3448-3442 cm^{-1}, and another group
342 of H-O-H bending vibrations at the range of wavenumber 1428-1415 cm^{-1}.

343 **O-H stretching vibration of MMWM.**

344 It is noted that the sharp intense band at 3643 cm^{-1} was overlapped with the broad
345 band of vibrations of water (Fig. 3a). This is attributed to O-H stretching vibrations
346 for the structural hydroxyl groups of MMWM (MM un-heated, MM 300, MM 400
347 and MM 500), which appeared at 3643 cm^{-1}. However, such O-H stretching vibrations
348 disappeared in the spectra of MMWM being thermal treated at temperatures higher
349 than 600 °C (MM 600, MM 700, MM 800, MM 900, and MM 1000). This suggests
350 that the structural O-H groups were retained in clay interlayers when thermal
351 treatment temperature was increased up to 600 °C, but they were removed when the
352 temperatures of thermal treatment were higher than 600 °C. A prominent broad band
353 of vibration of water could only be observed in MM un-heated and MM 300 with the
354 center at 3448-3442 cm^{-1} while the intensity of this band decreased significantly with
355 increasing temperatures. The loosely bonded water molecules in MMWM were
356 removed when heated to 400 °C, and then the structural hydroxyl groups were

357 removed when temperatures rose above 600 °C. These findings are consistent with
358 those reported by Elkhalifah et al. (2013) and Martinez et al. (2017).

359 **H-O-H bending vibration of MMWM**

360 When considering vibrations of water molecules (Fig. 3b), the changes of FTIR
361 spectra in both regions of O-H stretching and H-O-H bending were due to the
362 reduction of hydrogen bonded water molecules with increasing temperature during
363 thermal treatment, changing the surface properties from hydrophilic to hydrophobic.
364 This phenomenon was due to the reduction of water content in MMWM by losing
365 hydroxyl groups of hydrated interlayers. The FTIR spectrum of MMWM
366 dehydroxylated at the highest temperature (i.e. 1000 °C) in this study exhibits the
367 lowest band intensity in terms of more water molecules being released (see MM 1000
368 of Fig. 2).

369 In summary, the O-H stretching and H-O-H bending vibrations of hydrogen
370 bonded water in MMWM provide evidence for the change in surface affinity from
371 hydrophilic to hydrophobic (Rathnayake et al. 2017). This phenomenon of surface
372 variation from the dehydroxylation of MMWM could correspond to the increase in
373 adsorption capacity. We assume that the absence of infrared bands represents the
374 process in which MMWM performed partial to total loss of hydroxylation water due
375 to heating at different temperatures. This change in property of the MMWM as a
376 result of losses in water molecules, in particular those on the mineral surface, is an

377 important process to make the dehydroxylated MMWM a superior adsorbent over the
378 non-dehydroxylated MMWM. Calcination of MMWM at suitable temperatures can
379 certainly improve its adsorption capacity by removing the physically and chemically
380 bonded water molecules and turning the surface properties from hydrophilic into
381 hydrophobic. However, metal oxides that formed on the mineral surface at high
382 temperatures that were observed in this study, may reduce the adsorption capacity of
383 MMWM.

384 ***Morphological change observed by field emission scanning electron microscopy***
385 ***(FESEM)***

386 Figure 4 shows the FESEM images of MMWM before and after thermal treatment,
387 as well as the EDX results of MMWM prior to dehydroxylation. The bulk of the
388 material consists mainly of schistose substances with various particle sizes being
389 observed from Fig. 4(a & c) which are associated with blurry and lamellar layers
390 being found at a high amplification. Moreover these small schistose substances also
391 congregate into a rough surface as shown in Fig. 4(d). In addition, the area scanning
392 results of EDX displayed in Fig. 4(b) indicate that the MMWM sample shown in Fig.
393 4(a) (mainly containing Ca, Si, Al and Fe, apart from the organic components O and
394 C) are consistent with the results of ICP-OES. The MMWM used in this study is
395 mainly composed of clay minerals and its shape primarily presents a schistose
396 appearance. The images shown in Fig. 4(e-i) reflect the effects of thermal treatment
397 on the morphological changes of MMWM. The images in Fig. 4(e, f & g) show the

398 increases in amorphous particles that corresponded to thermal treatment temperatures
399 at 300, 400, and 500 ℃. Blurry edges and some cloud-like particles are also observed.
400 Meanwhile a number of crystals were separated into several pieces, like the
401 amorphous substances forming the poorly crystalline minerals in MMWM. When
402 MMWM was heated to 500 ℃, the MMWM mass clearly revealed small pieces of
403 schistose layers (less than 100 nm), composed mainly of granular and schistose
404 crystals. When the thermal treatment temperature was increased to 600 ℃ as seen in
405 Fig. 4(h), the surface morphology differed slightly as some crystalline particles were
406 forming due to recrystallization during phase transformation. The schistose
407 appearances became increasingly evident when the temperature was increased from
408 700 to 1000 ℃, and the schistose layers increased to larger than 500 nm (Fig. 4(i-l)).
409 This is probably due to the formation of new phases during transformation. It is
410 consistent with the results reported by Kremer et al. (2008). The external appearances
411 of the thermally treated MMWM samples heated at 600 ℃ and higher (Fig. 4 (h-l))
412 were different from those of non-dehydroxylated MMWM samples (Fig. 4 (a, c-d))
413 and dehydroxylated MMWM at lower temperatures (Fig. 4 (e-g)). The thermal
414 modification at the appropriate temperatures (e.g. 300-700 ℃) may provide a mass of
415 layers, rough surface and large surface area which would improve the adsorption
416 ability of MMWM.

417 ***Change in X-Ray diffraction (XRD) pattern***

418 Figure 5 displays the XRD patterns of MMWM before and after thermal treatment.
419 The reflections at 20.71° and 26.45° correspond to quartz detected in MMWM
420 samples (Fig. 5) and it can be used as an internal standard for d-spacing manipulation.
421 The peaks observed in the XRD patterns of MMWM were identified as a series of
422 minerals compared to the standard patterns. The mineral compositions of MMWM
423 used in this study include montmorillonite (Clay) (ICSD (00-002-0239), illite (ICSD
424 (00-002-0056)), kaolinite (ICSD 01-078-2110), muscovite (ICSD (00-002-0056)),
425 mica (ICSD (00-002-0051), feldspar (ICSD (01-08908575)), quartz (ICSD (00-046-
426 1045)), calcite (ICSD (00-005-0586)) and rectorite (allevardite) (ICSD (00-029-
427 1495)). The MMWM samples that consisted of a series of clay minerals reveal their
428 great potential ability in contaminant adsorption, most of which can be further
429 modified by sintering to achieve better adsorption capacity (Alvarez-ayuso and
430 Garcia-Sanchez 2003; Adebowale et al. 2008; Sen and Bhattacharyya 2008; Etci et al.
431 2010; Msaadi et al. 2017). All the peaks showed decreases in intensity with increasing
432 temperature, and then some small peaks disappeared as the temperature reached
433 900 ℃. Reflection of microcline (ICSD (00-019-0926)) at 27.08° was observed for
434 MM un-heated, MM 300, MM 400, MM 500, and MM 600 samples, but it
435 disappeared as temperatures reached 700 ℃. The reformation of mineral structures
436 during thermal treatment might contribute to the fading away of microcline. Two new
437 reflections at 30.02° and 31.33° with low intensity were observed in the spectrum of

438 MM 1000, which were attributed to the generation of magnesian gehlenite after
439 comparing with the standard pattern (ICSD (01-079-2422)). According to Traoré et al.
440 (2008), micro-composite microstructure at the micron scale is obtained by sintering
441 clay (kaolinite) and calcite at 1100 °C, where the formation of gehlenite occurs. The
442 sintering modification of MMWM resulted in the formation of new minerals at a high
443 temperature (1000 °C) but contributed less to adsorption ability. The study therefore
444 suggests that the improvement of adsorption ability of MMWM after thermal
445 treatment is seldom contributed by the crystal reformation.

446 ***Improvement of adsorption ability after modification***

447 ***Adsorption capacity of methyl orange***

448 The maximum amounts of MO adsorbed by MMWM samples heated at different
449 temperatures are plotted in Fig. 6. These MMWM samples showed various adsorption
450 abilities towards MO, changing from 24.9 to 87.6 mg/g, which minimized in the MM
451 1000 sample and maximized in the MM 400. The MMWM sample heated at 400 °C
452 showed a better MO adsorption capacity than those of bottom ash and de-oiled soya
453 from the soya oil industry with the adsorption capacity of each adsorbent being 3.61
454 and 16.66 mg/g, respectively (Mittal et al. 2007). According to Liu et al. (2011),
455 organic-montmorillonite adsorbent treated by microwave irradiation reaches a
456 maximum value of MO adsorption of approximately 50 mg/g. Our results indicated
457 that the adsorption capacity of MMWM on MO was increased by 28.43% from 68.21

458 to 87.60 mg/g with the increase in temperatures up to 400 ℃ during thermal treatment,
459 corresponded to a 59.61% enlargement of SSA at this temperature (Fig. 1). When the
460 thermal treatment temperature was increased to higher than 400 ℃, the adsorption
461 capacity showed a decreasing trend and minimized at 1000 ℃ with a value of 24.96
462 mg/L, which was only 28.5% of the value at 400 ℃. The MO adsorption capacity
463 followed a similar trend with the loss of structural O-H groups and the change in SSA,
464 suggesting that the adsorption of MO was mainly attributed to the functional groups
465 performing affinity of adsorption in the interlayers of dehydroxylated MMWM in
466 conjunction with the increase in SSA. The FTIR spectra of MM 400 before and after
467 MO adsorption were selected to be demonstrated in Fig. 7. Two new bands at 1633
468 and 3432 cm^{-1} were observed in the MO adsorbed MM 400, but the band at 3643 cm^{-1}
469 was overlapping and shifting to 3623 cm^{-1}. Referring to the band fitting for spectra of
470 Fig. 8 (a & b), the band at 3643 cm^{-1} cannot be found in the MO adsorbed MM 400,
471 whereas absorbance bands are found at 3623 and 3232-3230 cm^{-1}. Meanwhile, the
472 intensity of the band at 3435 cm^{-1} increases conspicuously after MO absorption. Fig.
473 8(d & e) demonstrates band fitting spectra of MM 400 before and after MO
474 adsorption in the range of 1750-1350 cm^{-1}. Three hidden bands are found in each
475 spectrum, bands at 1634 and 1462/1464 cm^{-1} remain unchanged but the band at 1434
476 cm^{-1} shifts to 1420 cm^{-1} after MO adsorption. The shift of vibrational frequency is
477 believed to be due to the change in surface property from hydrophobic to hydrophilic
478 after MO adsorption (Rathnayake et al. 2016). The disappearance of O-H stretching

479 vibration at 3643 cm^{-1} for the structural hydroxyl groups of MM 400 after MO
480 absorption is observed and comes with the appearance of a new vibration at 3435 cm^{-1}.
481 This phenomenon was caused by MO molecules bonded to the -OH group on the
482 interlayer of MM 400 surface, and the newly appeared vibration was contributed by
483 the MO molecule. Thus, adsorption of MO by dehydroxylated MMWM was mainly
484 contributed by combining MO molecules with the functional groups on mineral
485 surface, where more affinity sites were created during phase transformation resulting
486 from the dehydroxylation process. According to Chen et al. (2012), the adsorption of
487 MO onto heat-treated clay mineral is controlled by two mechanisms: hydrogen
488 bonding between oxygen groups of $-SO_3^-$ (anionic head of MO) and H^+ of coordinated
489 water (<300 ℃), and electrostatic interaction between dye and negatively charged
490 surface of heat-treated clay (>400 ℃). In conclusion, the enhancement of MO
491 adsorption capacity of thermally treated MMWM (e.g. MM 400) is caused by the
492 appearance of O-H groups after losing loosely bond water molecules and the
493 increasing surface area of dehydroxylated MMWM, during which the process of
494 hydrogen bonding is dominant (Chen et al. 2012). The gradual loss of structural
495 hydroxyl groups of dehydroxylated MMWM resulted in the decline of MO adsorption
496 ability from 65.24 to 24.96 mg/g when thermal treatment temperature was increased
497 from 500 to 1000 ℃, during which the process of electrostatic interaction was
498 dominant associated with the decrease in SSA of MMWM, showing a similar trend
499 identical to the variation of temperature (Chen et al. 2012). In addition, the SEM (Fig.

4) results show that the structure of MM 400 is looser, which could facilitate the adsorption of MO onto surface (Liu et al. 2011). Hence, the increase or decrease in MO adsorption capacity of dehydroxylated MMWM are contributed by both the changes in surface properties such as SSA and morphology and phase transformation during dehydroxylation at different stages of thermal treatment corresponding to heating temperature.

The amounts of MO adsorbed by the MMWM heated at 400 ℃ as a function of adsorption time is shown in Fig. 9. The MO adsorption onto MM 400 increased rapidly during the first 100 minutes and then slowed down until MO adsorption reached 87.6 mg/g after 420 mins, where the adsorption equilibrium point was achieved. The equilibrium uptake per unit mass of the adsorbent was higher than bentonite (6.7 mg/g) but lower than palygorskite (95.9 mg/g) (Chen et al. 2012; Leodopoulos et al. 2012). Compared with the organic-montmorillonite (49.8 mg/g) pre-treated by microwave irradiation, MM 400 showed a shorter equilibrium time and doubled the adsorption capacity (Liu et al. 2011). The adsorption curve was fitted by using the pseudo-second-order model. The corresponding parameters and correlation coefficient (R^2) showed that the experimental data were well fitted to the pseudo-second-order kinetic model with $R^2 = 0.994$, suggesting that the MO adsorption onto MM 400 is chemisorption dominated. According to Chen et al. (2012), a pseudo-second-order model provided the best correlation of the experimental kinetic data to

the MO adsorption of clay mineral. This is also consistent with the previous results from FTIR spectra of MMWM in this study.

Figure 10 shows the Langmuir and Freundlich adsorption isotherms of MM 400 in the solution with various initial MO concentrations at room temperature (25 ℃). A high correlation coefficient (R^2 = 0.964) was derived from the fitting data of adsorption experiment into the Langmuir isotherm model, as well as the comparison with that of the Freundlich isotherm model (R^2 = 0.724). This suggests that the observed feature of adsorption onto MM 400 can be assigned to monolayer coverage. Similar results for heat-treated clay minerals were reported by Chen et al. (2012) and Luo et al. (2015), in which the adsorption isotherms of MO onto clays could be best described by the Langmuir equation.

Adsorption capacity of Lead

The amounts of Pb adsorbed by MMWM samples at 25 ℃ before and after thermal treatment at different temperatures are plotted in Fig. 11. The MMWM samples showed various adsorption abilities towards Pb adsorption, increasing from 349.3 (un-heated) to 518.9 mg/g when the treatment temperature was increased to 600 ℃. However, the adsorption capacity then decreased to 45.5 mg/g when heating temperature was increased up to 1000 ℃, where the reformation of crystal structures occurred. The MMWM sample heated at 600 ℃ (MM 600) showed much better Pb adsorption capacity than those of the adsorbents prepared from industrial wastes (blast

furnace sludge, 227 mg/g) and clay minerals (acid-activated kaolinite (6.3 mg/g) and acid-activated montmorillonite (22.7 mg/g)) (Bhatnagar et al. 2006; Gupta and Bhattacharyya 2005). In addition, the MM 600 showed greater adsorption capacity than those of natural goethite (109.2 mg/g), modified illite (239 mg/g), kaolinite (82.65 mg/g) and activated-montmorillonite (31.3 mg/g) (Alvarez-ayuso and Garcia-Sanchez 2003; Ozdes et al. 2011; Lounis et al. 2012). The EDX results of MM 600 after Pb adsorption is exhibited in Fig. 12, where Pb is observed as the second most abundant element (W: 37.4%) on the MMWM surface. The study suggests that the adsorption of Pb on MMWM was mainly performed by surface adsorption, and the variations in Pb adsorption capacity can be attributed to the enlarged surface area where more adsorption sites could have been provided. This is associated with the changes in surface property where variations in bonding were due to the performance of functional groups and to the alteration in surface charges and porosity related to phase transformation of minerals during the process of dehydroxylation.

The Pb adsorption capacity of the heated MMWM sample (MM 600) as a function of adsorption time is shown in Fig. 13. The Pb adsorption onto MM 600 increased rapidly during the first 80 minutes and then changed gradually until the amount of Pb adsorbed reached 510 mg/g after 420 mins, where the adsorption equilibrium was attained. As the adsorption kinetics were described using the pseudo-second-order model, the corresponding parameters and correlation coefficient (R^2) showed that the experimental data were well fitted to the pseudo-second-order kinetic

561 model with R^2 = 0.941, suggesting that the Pb adsorption onto MM 600 was
562 chemisorption. This is consistent with the previous results in this study that MM 600
563 can adsorb a large amount of Pb onto its surface although the surface area of MMWM
564 is rather small. This could be attributed to the increase in negative charges on the
565 lattice of the mineral surface, especially during the process of dehydroxylation,
566 dominating the adsorption. Moreover, the rate constant *k* of the pseudo-second-order
567 fitting plot of MM 600 was 0.0375 g mg^{-1} min^{-1}, which is close to that of kaolinite
568 (0.035 g mg^{-1} min^{-1}) but smaller than that of montmorillonite (0.084 g mg^{-1} min^{-1})
569 (Naseem and Tahir 2001). Therefore, MM 600 exhibited a dramatically enhanced Pb
570 removal performance, including much higher Pb adsorption capacity and faster
571 adsorption with a high adsorption rate. Herein, MM 600 was chosen for further Pb
572 adsorption isotherm study.

573 Figure 14 shows the Langmuir and Freundlich Pb adsorption isotherms of MM 600
574 in various initial concentrations in solution at room temperature (25 °C). A high
575 correlation coefficient (R^2 = 0.971) was derived from fitting the experimental
576 adsorption data into the Langmuir isotherm model, as well as a comparison with the
577 Freundlich isotherm model (R^2 = 0.881). This suggests that the observed feature of
578 adsorption onto MM 600 can be assigned to monolayer coverage, which is in
579 agreement with the previous findings that the interaction between Pb and the schistose
580 adsorbent is endothermic in nature (Frost et al. 2004). Moreover, MM 600 possessed a
581 considerable adsorption capacity compared to other clay minerals (acid-activated

582 montmorillonite, 22.7 mg/g; beidellite, 86.9 mg/g) or mixed metal-modified clay
583 mineral adsorbents (Zn-imprinted polymer/montmorillonite, 301 mg/g) (Etci et al.
584 2010; Msaadi et al. 2017).

585 # Implications

586 Modification on the properties of MMWM to increase its adsorption capacity can
587 be achieved by thermal treatment. Property characterization revealed that the changes
588 in surface morphology of MMWM can be clearly observed at different stages of the
589 thermal process. Different levels of phase transformation are related to the variations
590 in mineral properties of MMWM as affected by dehydroxylation. The capacities of
591 MMWM on adsorption of MO (MM 400, 87.60 mg/g) and Pb (MM 600, 514 mg/g)
592 have been successfully optimized after thermal modification. The increase in
593 adsorption capacity is attributed to the enlarged SSA where more adsorption sites
594 were generated, to the change in surface property where variation of bonding is due to
595 the performance of functional groups, and to the alteration of surface charge. The MO
596 and Pb adsorption curves of MMWM can be well fitted to the pseudo-second-order
597 kinetic model, to which the MO and Pb adsorptions by MMWM are mainly
598 chemisorption. Adsorption isotherms are better fitted to the Langmuir model than to
599 the Freundlich one, suggesting that adsorptions of MO and Pb onto MMWM could be
600 assigned to monolayer coverage. Thus, thermally treated MMWM is confirmed to be
601 a good adsorbent for the removal of contaminants, especially for Pb in solution. The

602 results of this study may provide information for the production of adsorbent derived
603 from mineral waste material that can be applied to environmental remediation and
604 useful to the integrated management of solid waste materials.

605 Acknowledgement

606 This research was financially supported by the Beijing Normal University-Hong
607 Kong University United International College (UIC), under the Research Project
608 R201710 and the Zhuhai Key Laboratory Research Fund R1053. The XRD and
609 FESEM used in this work was supported by the Institute of Advanced Materials (IAM)
610 with funding from the Special Equipment Grant from the University Grants
611 Committee of the Hong Kong Special Administrative Region, China (SEG_HKBU06))

612 References cited

613 Adebowale, K.O., Unuabonah, E.I., and Olu-Owolabi, B.I. (2008) Kinetic and
614 thermodynamic aspects of the adsorption of Pb 2+, and Cd 2+, ions on
615 tripolyphosphate-modified kaolinite clay. Chemical Engineering Journal, 136,
616 99-107. https://doi.org/10.1016/j.cej.2007.03.012
617 Alvarez-Ayuso, E., and Garćia-Sánchez, A. (2003) Removal of heavy metals from
618 waste waters by natural and Na-exchanged bentonites. Clays and Clay minerals,
619 51, 475-480. https://doi.org/10.1346/CCMN.2003.0510501
620 Belzunces, B., Hoyau, S., Benoit, M., Tarrat, N., and Bessac, F. (2017) Theoretical
621 study of the atrazine pesticide interaction with pyrophyllite and Ca^{2+}-

montmorillonite clay surfaces. Journal of Computational Chemistry, 38, 133-143. https://doi.org/10.1002/jcc.24530

Bhatnagar, A., Jain, A. K., Minocha, A. K., and Singh, S. (2006) Removal of lead ions from aqueous solutions by different types of industrial waste materials: equilibrium and kinetic studies. Separation Science and Technology, 41, 1881-1892. https://doi.org/10.1080/01496390600725828

Bhattacharyya, K. G., and Gupta, S. S. (2008) Adsorption of a few heavy metals on natural and modified kaolinite and montmorillonite: a review. Advances in Colloid and Interface Science, 140, 114-131. https://doi.org/10.1016/j.cis.2007.12.008

Brown, G. and Brindley, G.W. (1982) X-ray diffraction procedures for clay mineral identification. In Brown, G. Ed., Crystal structures of clay minerals and their X-ray identification, p. 197-248. The Mineralogical Society of Great Britain and Ireland.

Chen, H., Zhong, A., Wu, J., Zhao, J., and Yan, H. (2012) Adsorption behaviors and mechanisms of methyl orange on heat-treated palygorskite clays. Industrial & Engineering Chemistry Research, 51, 14026–14036. https://doi.org/10.1021/ie300702j

Csáki, Š., Trnovcová, V., Štubňa, I., Ondruška, J., Sunitrová, I., Vozár, L., and Dobroň, P. (2017) AC conductivity of an illitic clay with zeolite addition after firing at different temperatures. Proceeding of AIP Conference Proceedings 1866, p. 040008. American Institute of Physics. https://doi.org/10.1063/1.4994488

Da Silva, G.J., Fossum, J.O., DiMasi, E., and Måløy, K.J. (2003) Hydration transitions in a nanolayered synthetic silicate: A synchrotron x-ray scattering study. Physical Review B, 67, 94-114. https://doi.org/10.1103/PhysRevB.67.094114

649 De Oliveira, T., Guégan, R., Thiebault, T., Le Milbeau, C., Muller, F., Teixeira, V.,
650 and Boussafir, M. (2017) Adsorption of diclofenac onto organoclays: Effects of
651 surfactant and environmental (pH and temperature) conditions. Journal of
652 hazardous materials, 323, 558-566.
653 https://doi.org/10.1016/j.jhazmat.2016.05.001
654 Eljiedi, A.A.A., and Kamari, A. (2017) Removal of methyl orange and methylene
655 blue dyes from aqueous solution using lala clam (Orbicularia orbiculata) shell.
656 Proceeding of AIP Conference Proceedings, 1847, p. 040003. American
657 Institute of Physics. https://doi.org/10.1063/1.4983899
658 Elkhalifah, A.E., Bustam, M.A., and Murugesan, T. (2013) Thermal properties of
659 different transition metal forms of montmorillonite intercalated with mono-, di-,
660 and triethanol ammonium compounds. Journal of Thermal Analysis and
661 Calorimetry, 112, 929-935. https://doi.org/10.1007/s10973-012-2657-z
662 Etci, Ö., Bektaş, N., and Öncel, M. S. (2010) Single and binary adsorption of lead and
663 cadmium ions from aqueous solution using the clay mineral beidellite.
664 Environmental Earth Sciences, 61, 231-240. https://doi.org/10.1007/s12665-
665 009-0338-4
666 Fonseca, C.G., Vaiss, V.S., Wypych, F., Diniz, R., and Leitão, A.A. (2017) Structural
667 and thermodynamic investigation of the hydration-dehydroxylation
668 dehydroxylation process of Na^{+}-montmorillonite using DFT calculations.
669 Applied Clay Science, 143, 212-219.
670 https://doi.org/10.1016/j.clay.2017.03.025
671 Fouodjouo, M., Fotouo-Nkaffo, H., Laminsi, S., Cassini, F.A., de Brito-Benetoli, L.O.,
672 and Debacher, N.A. (2017) Adsorption of copper (II) onto cameroonian clay
673 modified by non-thermal plasma: Characterization, chemical equilibrium and
674 thermodynamic studies. Applied Clay Science. 142, 136-144.
675 https://doi.org/10.1016/j.clay.2016.09.028

676 Frost, R.L., Horváth, E., Makó, É., and Kristóf, J. (2004) Modification of low-and
677 high-defect kaolinite surfaces: implications for kaolinite mineral processing.
678 Journal of Colloid and Interface Science, 270, 337-346.
679 https://doi.org/10.1016/j.jcis.2003.10.034
680 Freundlich, H. (1907) Über die adsorption in lösungen. Zeitschrift für physikalische
681 Chemie, 57, 385-470. https://doi.org/10.1515/zpch-1907-5723
682 GuccnNnnrtr, S., Cn, Y.H., and Van Gnoos, L.A.K. (1987) Muscovite
683 dehydroxylation: High-temperature studies. American Mineralogist, 72, 537-
684 550.
685 Gupta, S.S., and Bhattacharyya, K.G. (2005) Interaction of metal ions with clays: I. A
686 case study with Pb (II). Applied Clay Science, 30, 199-208.
687 https://doi.org/10.1016/j.clay.2005.03.008
688 Habiba, U., Siddique, T.A., Joo, T.C., Salleh, A., Ang, B.C., and Afifi, A.M. (2017)
689 Synthesis of chitosan/polyvinyl alcohol/zeolite composite for removal of
690 methyl orange, Congo red and chromium (VI) by flocculation/adsorption.
691 Carbohydrate Polymers, 157, 1568-1576.
692 https://doi.org/10.1016/j.carbpol.2016.11.037
693 Húlan, T., Trník, A., and Medveď, I. (2017) Kinetics of thermal expansion of illite-
694 based ceramics in the dehydroxylation region during heating. Journal of
695 Thermal Analysis and Calorimetry, 127, 291-298.
696 https://doi.org/10.1007/s10973-016-5873-0
697 Hurlbut, C.S., and Klein, C. (1977) Manual of Mineralogy (after James D. Dana).
698 Wiley. pp. 429
699 Jaramillo-Páez, C., Navío, J.A., Hidalgo, M.C., Bouziani, A., and El Azzouzi, M.
700 (2017) Mixed α-Fe2O/Bi2 WO 6 oxides for photoassisted hetero-Fenton
701 degradation of methyl orange and phenol. Journal of Photochemistry and
702 Photobiology A: Chemistry, 332, 521-533.
703 https://doi.org/10.1016/j.jphotochem.2016.09.031

Jiang, Y.N., Ruan, H.D., Lai, S.Y., Lee, C.H., Yu, C.F., Wu, Z., and He, S. (2013a) Recycling of solid waste material in Hong Kong: I. Properties of modified clay mineral waste material and its application for removal of cadmium in water. Earth Science, 2, 40-46. https://doi.org/10.11648/j.earth.20130202.13

Jiang, Y.N., Ruan, H.D., Zhang, G.F., Lai, S.Y., Lee, C.H., Yu, C.F., and He, S. (2013b) Recycling of solid waste material: II. phosphate adsorption by modified clay mineral waste material relating to remediation of eutrophication in aquatic systems. Proceedings of International Congress on Engineering and Information, p. 42. Hong Kong SAR.

Jiang, Y.N., Su, L.C., Ruan, H.D., Zhang, G.F., Lai, S.Y., Lee, C.H., and He, S. (2014) Adsorption of phosphorus by modified clay mineral waste material relating to removal of it from aquatic system. International Journal of Environmental Monitoring and Analysis, 2, 36-44. https://doi.org/10.11648/j.ijema.20140201.14

Kelley, F.R. (1957) Field Trip to the Ione Clay Area1 Held in Conjunction with the sixth national clay conference August 21, 1957. Clays and Clay Minerals, 6, 1-17. https://doi.org/10.1346/CCMN.1957.0060102

Kremer, B., Kazmierczak, J., and Stal, L.J. (2008) Calcium carbonate precipitation in cyanobacterial mats from sandy tidal flats of the North Sea. Geobiology, 6, 46-56.

Krupskaya, V.V., Zakusin, S.V., Tyupina, E.A., Dorzhieva, O.V., Zhukhlistov, A.P., Belousov, P.E., and Timofeeva, M.N. (2017) Experimental study of montmorillonite structure and transformation of its properties under treatment with inorganic acid solutions. Minerals, 7, 49. https://doi.org/10.3390/min7040049

Lagergren, S. (1898) Zur theorie der sogenannten adsorption geloster stoffe. Kungliga svenska vetenskapsakademiens. Handlingar, 24, 1-39.

731 Langmuir, I. (1916) The constitution and fundamental properties of solids and liquids.
732 Part I. Solids. Journal of the American Chemical Society, 38, 2221-2295.
733 https://doi.org/10.1021/ja02268a002
734 Langmuir, I. (1917) The constitution and fundamental properties of solids and liquids.
735 II. Liquids. Journal of the American Chemical Society, 39, 1848-1906.
736 https://doi.org/10.1021/ja02254a006
737 Leodopoulos, C., Doulia, D., Gimouhopoulos, K., and Triantis, T.M. (2012) Single
738 and simultaneous adsorption of methyl orange and humic acid onto bentonite.
739 Applied Clay Science, 70, 84-90. https://doi.org/10.1016/j.clay.2012.08.005
740 Liu, B., Wang, X., Yang, B., and Sun, R. (2011) Rapid modification of
741 montmorillonite with novel cationic Gemini surfactants and its adsorption for
742 methyl orange. Materials Chemistry and Physics, 130, 1220-1226.
743 https://doi.org/10.1016/j.matchemphys.2011.08.064
744 Lounis, Z., Saddouki, S., and Djafri, F. (2012) Removal of Pb2+ ions in aqueous
745 phase by a sodic montmorillonite. Journal of Analytical Science & Technology,
746 3, 104-112. https://doi.org/10.5355/JAST.2012.104
747 Lu, H.R., Su, L.C., and Ruan, H.D. (2016) Removal of Pb, Cd, and Cr in a water
748 purification system using modified mineral waste materials and activated
749 carbon derived from waste materials. Proceeding of IOP Conference Series:
750 Earth and Environmental Science. 39, p. 1755-1315. IOP Publishing.
751 https://doi.org/10.1088/1755-1315/39/1/012005
752 Luo, Z., Gao, M., Ye, Y., and Yang, S. (2015) Modification of reduced-charge
753 montmorillonites by a series of gemini surfactants: characterization and
754 application in methyl orange removal. Applied Surface Science, 324, 807-816.
755 https://doi.org/10.1016/j.apsusc.2014.11.043
756 Martinez, J.M., Volzone, C., and Garrido, L.B. (2017) Thermal transformations up to
757 1200° C of Al-pillared montmorillonite precursors prepared by different OH–

758 Al polymers. Journal of Thermal Analysis and Calorimetry, 128, 61-69.
759 https://doi.org/10.1007/s10973-016-5938-0
760 Miller, J.G., and Oulton, T.D. (1970) Prototropy in kaolinite during percussive
761 grinding. Clays Clay Minerals, 18, 313-23.
762 https://doi.org/10.1346/CCMN.1970.0180603
763 Mittal, A., Malviya, A., Kaur, D., Mittal, J., and Kurup, L. (2007) Studies on the
764 adsorption kinetics and isotherms for the removal and recovery of Methyl
765 Orange from wastewaters using waste materials. Journal of Hazardous
766 Materials, 148, 229-240. https://doi.org/10.1016/j.jhazmat.2007.02.028
767 Msaadi, R., Ammar, S., Chehimi, M.M., and Yagci, Y. (2017) Diazonium-based ion-
768 imprinted polymer/clay nanocomposite for the selective extraction of lead (ii)
769 ions in aqueous media. European Polymer Journal, 89, 367-380.
770 https://doi.org/10.1016/j.eurpolymj.2017.02.029
771 Naseem, R., and Tahir, S.S. (2001) Removal of Pb (II) from aqueous/acidic solutions
772 by using bentonite as an adsorbent. Water Research, 35(16), 3982-3986.
773 https://doi.org/10.1016/S0043-1354(01)00130-0
774 Ozdes, D., Duran, C., and Senturk, H.B. (2011) Adsorptive removal of Cd(ii) and
775 pb(ii) ions from aqueous solutions by using turkish illitic clay. Journal of
776 Environmental Management, 92, 3082-90.
777 https://doi.org/10.1016/j.jenvman.2011.07.022
778 Rathnayake, S. I., Xi, Y., Frost, R. L., and Ayoko, G. A. (2016) Environmental
779 applications of inorganic–organic clays for recalcitrant organic pollutants
780 removal: Bisphenol A. Journal of Colloid and Interface Science, 470, 183-195.
781 https://doi.org/10.1016/j.jcis.2016.02.034
782 Rathnayake, S.I., Martens, W.N., Xi, Y., Frost, R.L., and Ayoko, G.A. (2017)
783 Remediation of Cr (VI) by inorganic-organic clay. Journal of Cand Interface
784 Science, 490, 163-173. https://doi.org/10.1016/j.jcis.2016.11.070

785 Richards, S., and Bouazza, A. (2007) Phenol adsorption in organo-modified basaltic
786 clay and bentonite. Applied Clay Science, 37, 133-142.
787 https://doi.org/10.1016/j.clay.2006.11.006
788 Ruan, H.D. and Gilkes, R.J. (1996) Kinetics of thermal dehydroxylation of synthetic
789 aluminous goethite. Journal of Thermal Analysis. 46, 1223-1238.
790 https://doi.org/10.1007/BF01979237
791 Schultz, L.G. (1969) Lithium and potassium absorption, dehydroxylation temperature,
792 and structural water content of aluminous smectites. Clays and Clay Minerals,
793 17, 115-149.
794 Srodon, J., and Eberl, D.D. (1984) Illite. Reviews in Mineralogy and Geochemistry,
795 13, 495-544. https://doi.org/10.1346/CCMN.1969.0170302
796 Sen, G.S., and Bhattacharyya, K.G. (2008) Immobilization of Pb(ii), Cd(ii) and Ni(ii)
797 ions on kaolinite and montmorillonite surfaces from aqueous medium. Journal
798 of Environmental Management, 87, 46-58.
799 https://doi.org/10.1016/j.jenvman.2007.01.048
800 Su, H., Fang, Z., Tsang, P.E., Fang, J., and Zhao, D. (2016) Stabilisation of nanoscale
801 zero-valent iron with biochar for enhanced transport and in-situ remediation of
802 hexavalent chromium in soil. Environmental Pollution, 214, 94-100.
803 https://doi.org/10.1016/j.envpol.2016.03.072
804 Takahashi, H. (1959) Effects of dry grinding on kaolin minerals. I. kaolinite. Bulletin
805 of the Chemical Society of Japan, 32, 235-245.
806 https://doi.org/10.1246/bcsj.32.235
807 Tambach, T.J., Hensen, E.J., and Smit, B. (2004) Molecular simulations of swelling
808 clay minerals. The Journal of Physical Chemistry B, 108, 7586-7596.
809 https://doi.org/10.1021/jp049799h
810 TraorÉ, K., KabrÉ, T.S., and Blanchart, P. (2003) Gehlenite and anorthite
811 crystallisation from kaolinite and calcite mix. Ceramics International, 29, 377-
812 383. https://doi.org/10.1016/S0272-8842(02)00148-7

813 Wang, X.L., Shen, J., Niu, Y.X., Wang, Y.G., Liu, G., and Sheng, Q.T. (2017)
814 Removal of phenol by powdered activated carbon prepared from coal
815 gasification tar residue. Environmental Technology, 39, 694-701.
816 https://doi.org/10.1080/09593330.2017.1310304
817 Yao, W., Yu, S., Wang, J., Zou, Y., Lu, S., Ai, Y., and Wang, X. (2017) Enhanced
818 removal of methyl orange on calcined glycerol-modified nano-crystallized
819 Mg/Al layered double hydroxides. Chemical Engineering Journal, 307, 476-
820 486. https://doi.org/10.1016/j.cej.2016.08.117
821 Zhao, Q., and Burns, S.E. (2013) Modeling sorption and diffusion of organic sorbate
822 in hexadecyltrimethylammonium-modified clay nanopores–a molecular
823 dynamics simulation study. Environmental science & technology, 47, 2769-
824 2776. https://doi.org/10.1021/es3045482

825 # Table

826 Table 1. Metal content of MMWM

	Ca	Fe	Al	Mg	Ti	Mn	Sr	Zn	Rb	Ba	Cu	Other
%	74.87	11.52	8.64	3.67	0.62	0.31	0.08	0.06	0.05	0.04	0.03	0.10

827

This is a preprint, the final version is subject to change, of the American Mineralogist (MSA)
Cite as Authors (Year) Title. American Mineralogist, in press.
DOI: https://doi.org/10.2138/am-2020-7227

828 # Figures

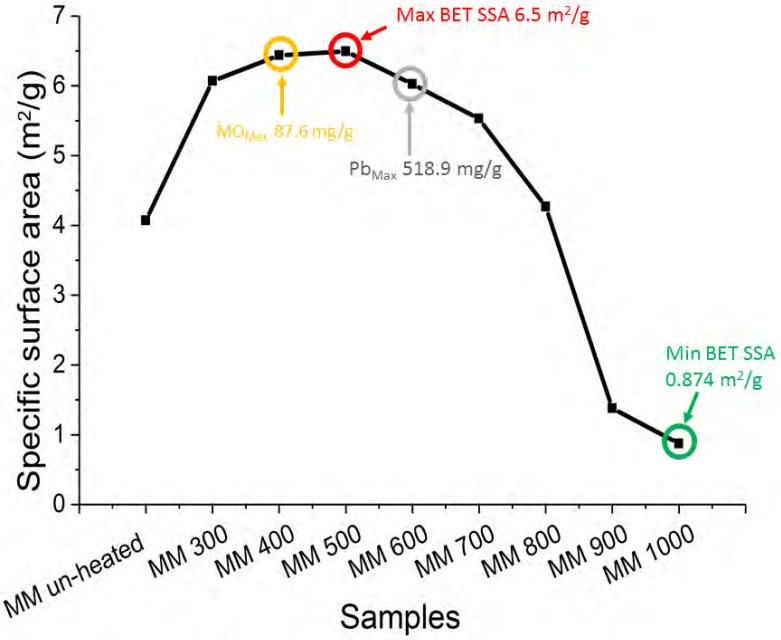

829
830 Figure 1 BET SSA of MMWM heated at different temperatures.

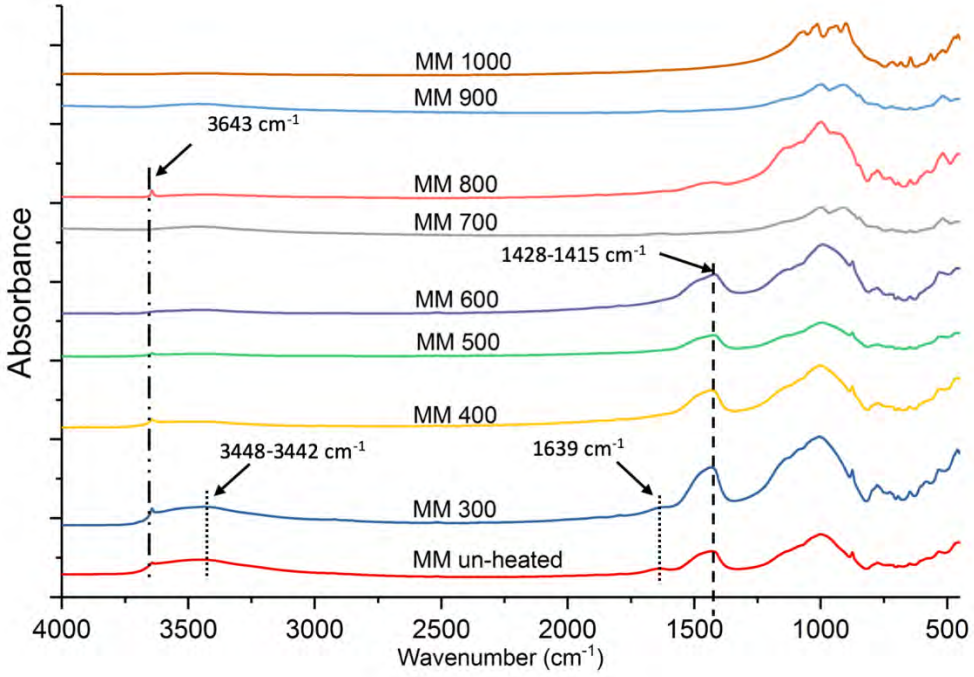

831
832 Figure 2 FTIR spectra of thermally treated MMWM at different temperatures in
833 the vibrational range of 4000-450 cm^{-1}
834

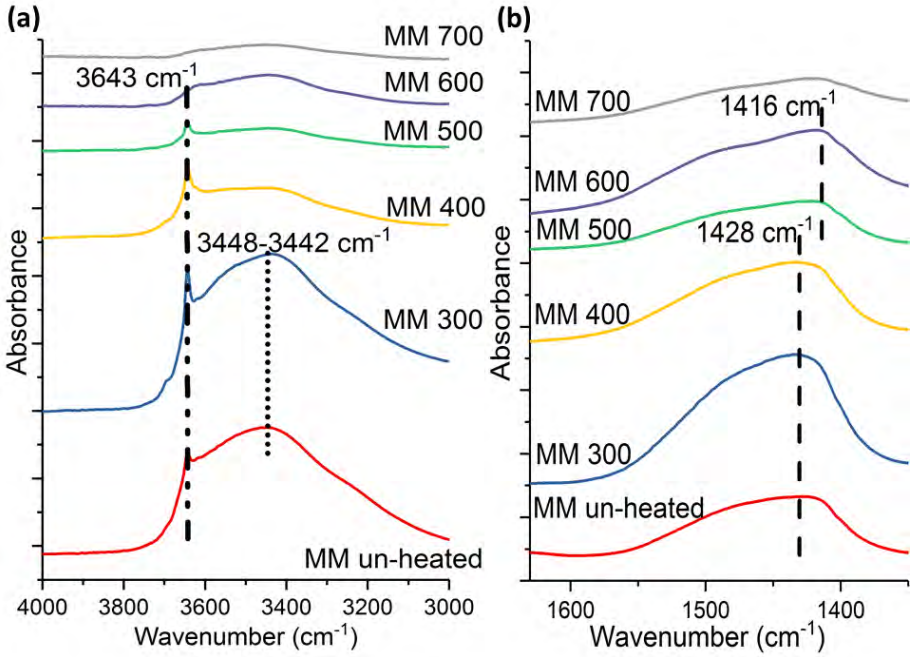

835
836 Figure 3 FTIR spectra of thermally treated MMWM at different temperatures, (a)
837 spectra in the range of 4000-3000 cm^{-1}; (b) spectra in the range of 1650-1350 cm^{-1}
838

This is a preprint, the final version is subject to change, of the American Mineralogist (MSA)
Cite as Authors (Year) Title. American Mineralogist, in press.
DOI: https://doi.org/10.2138/am-2020-7227

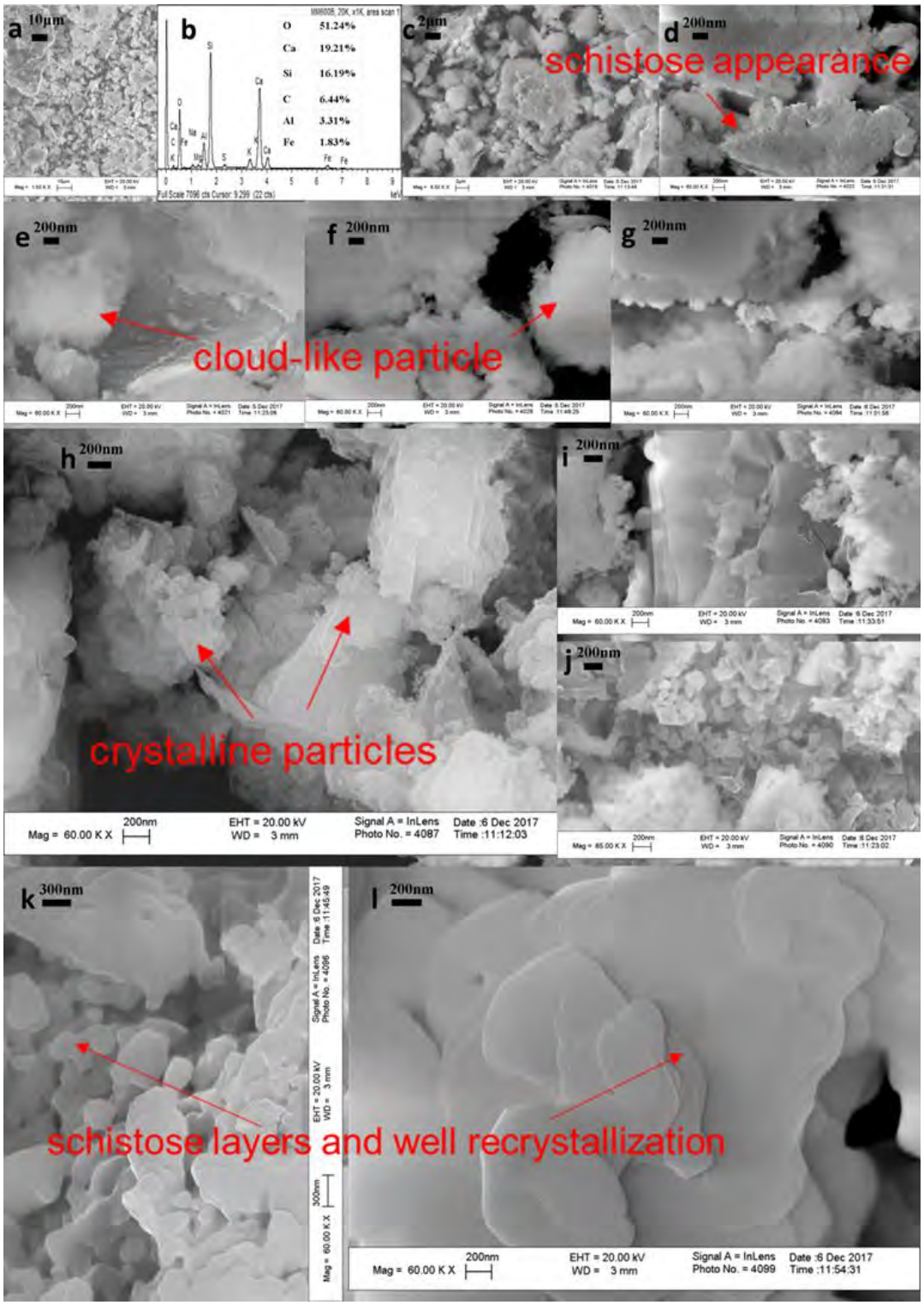

Figure 4 FESEM images of MM un-heated (a (1.5 K X), b (EDX), c (6.5 K X), d (60.0 K X)) and MMWM after thermal treatment at 300 °C (e), 400 °C (f), 500 °C (g), 600 °C (h), 700 °C (i), 800 °C (j), 900 °C (k), and 1000 °C (l)

This is a preprint, the final version is subject to change, of the American Mineralogist (MSA)
Cite as Authors (Year) Title. American Mineralogist, in press.
DOI: https://doi.org/10.2138/am-2020-7227

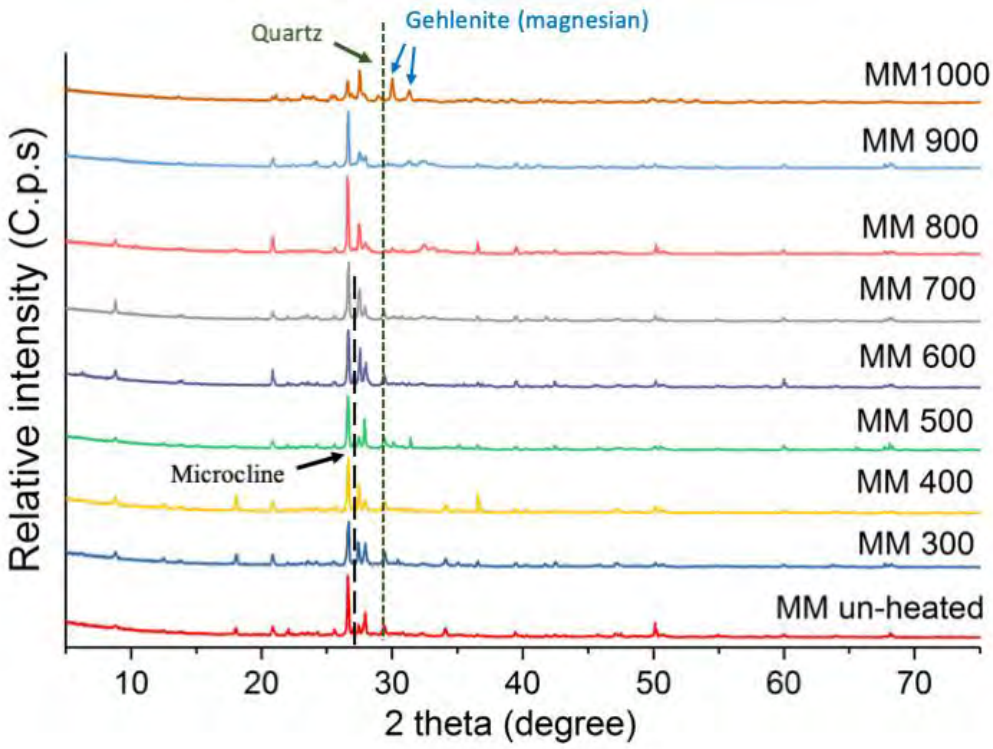

844

845 Figure 5 XRD patterns of MMWM before (MM un-heated) and after (MM 300-
846 1000) thermal treatment.

847

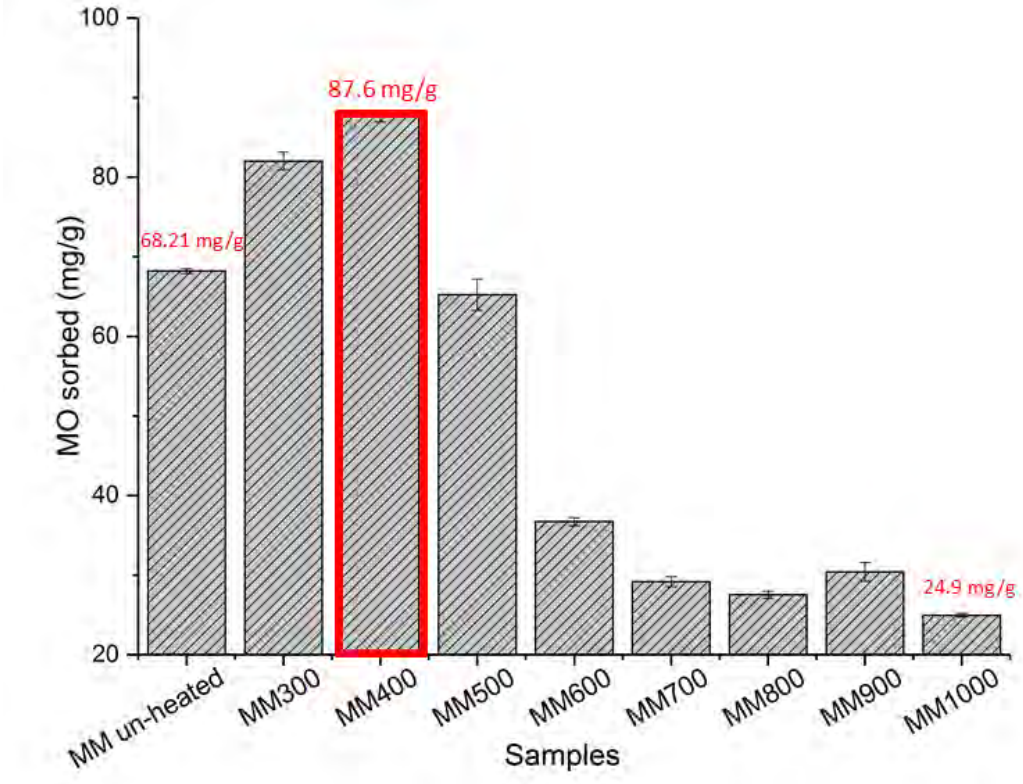

848

849 Figure 6 The maximum amounts of MO adsorbed by MMWM samples at 25 °C
850 before (MM un-heated) and after (MM 300-1000) thermal treatment

This is a preprint, the final version is subject to change, of the American Mineralogist (MSA)
Cite as Authors (Year) Title. American Mineralogist, in press.
DOI: https://doi.org/10.2138/am-2020-7227

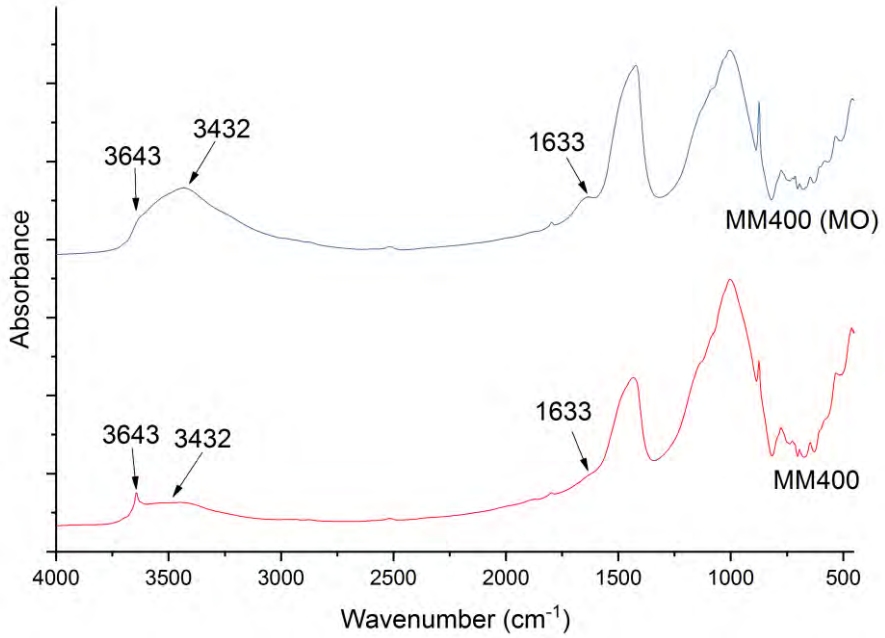

Figure 7 Comparison on the FTIR spectra of MM 400 before and after methyl orange (MO) adsorption

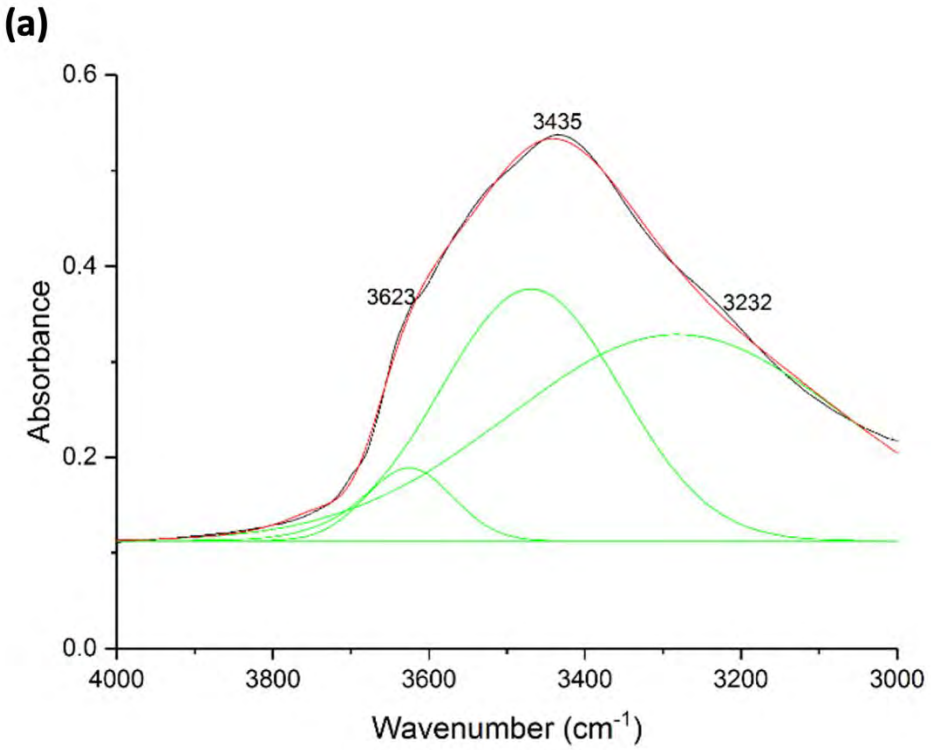

854

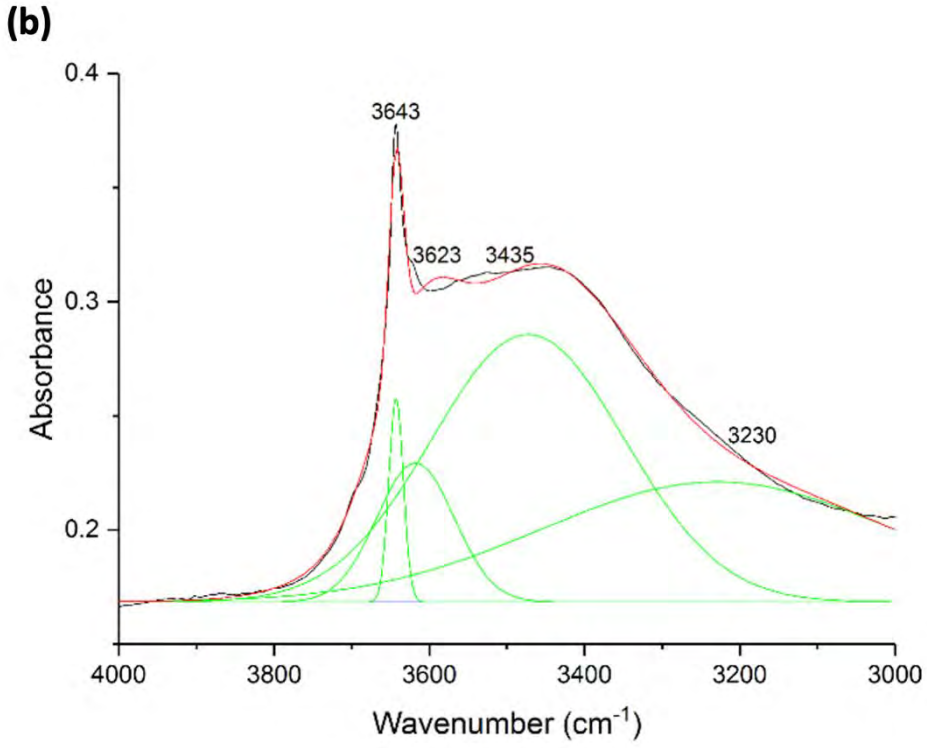

855

This is a preprint, the final version is subject to change, of the American Mineralogist (MSA)
Cite as Authors (Year) Title. American Mineralogist, in press.
DOI: https://doi.org/10.2138/am-2020-7227

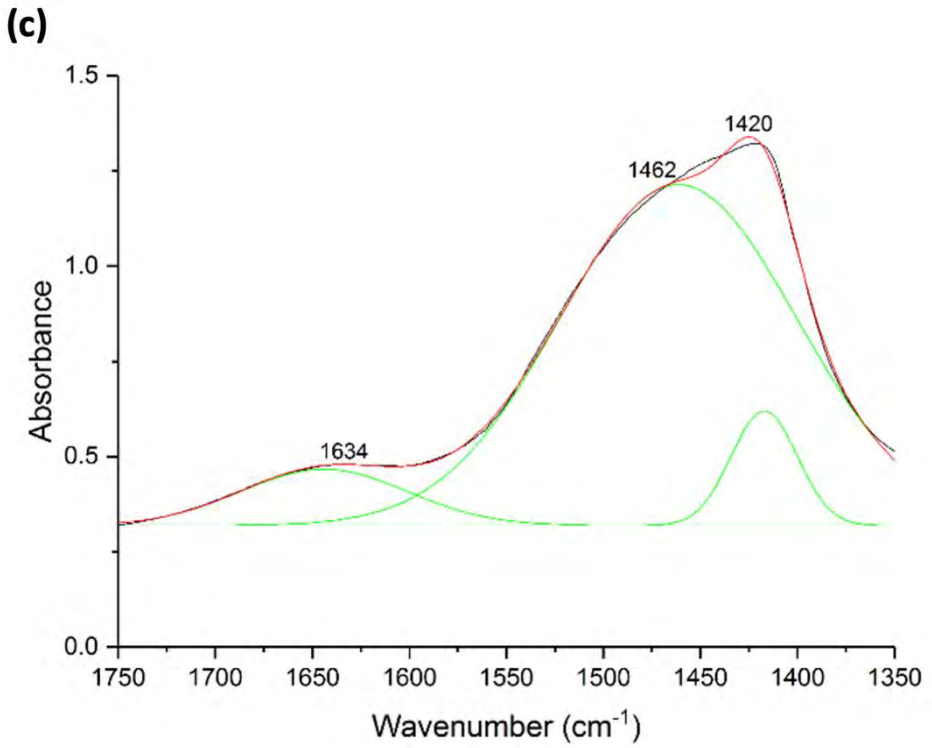

856

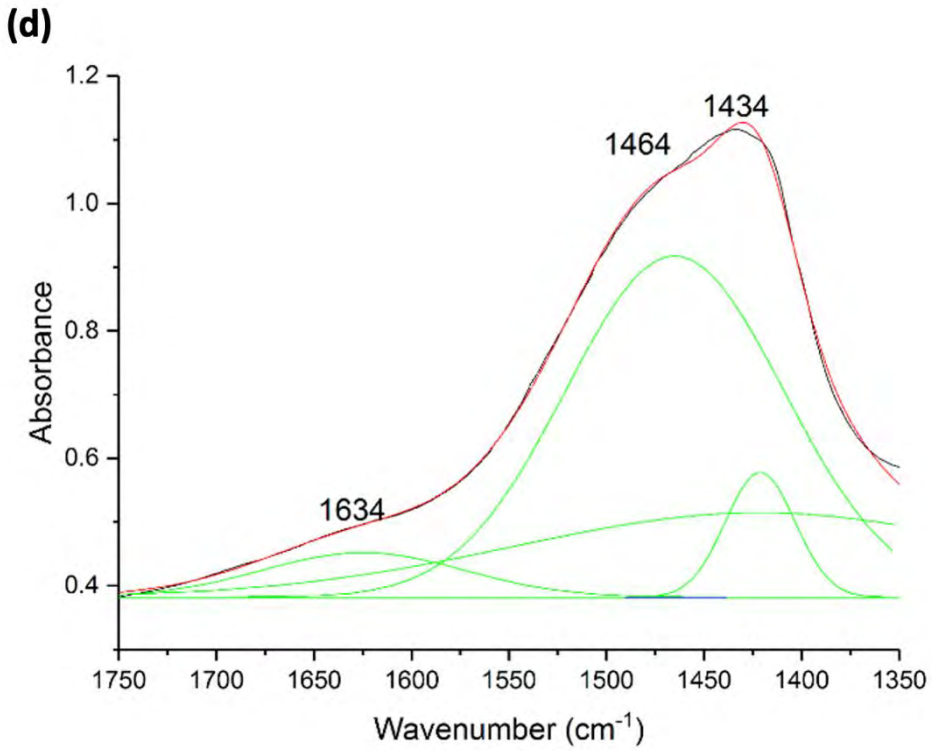

857

858 Figure 8 Band fittings of FTIR spectra, (a) MM 400 after MO adsorption, and (b)
859 MM 400 before adsorption in the range of 4000-3000 cm^{-1}; (c) MM 400 after MO
860 adsorption, and (d) MM 400 before adsorption in the range of 1750-1350cm^{-1}

861

This is a preprint, the final version is subject to change, of the American Mineralogist (MSA)
Cite as Authors (Year) Title. American Mineralogist, in press.
DOI: https://doi.org/10.2138/am-2020-7227

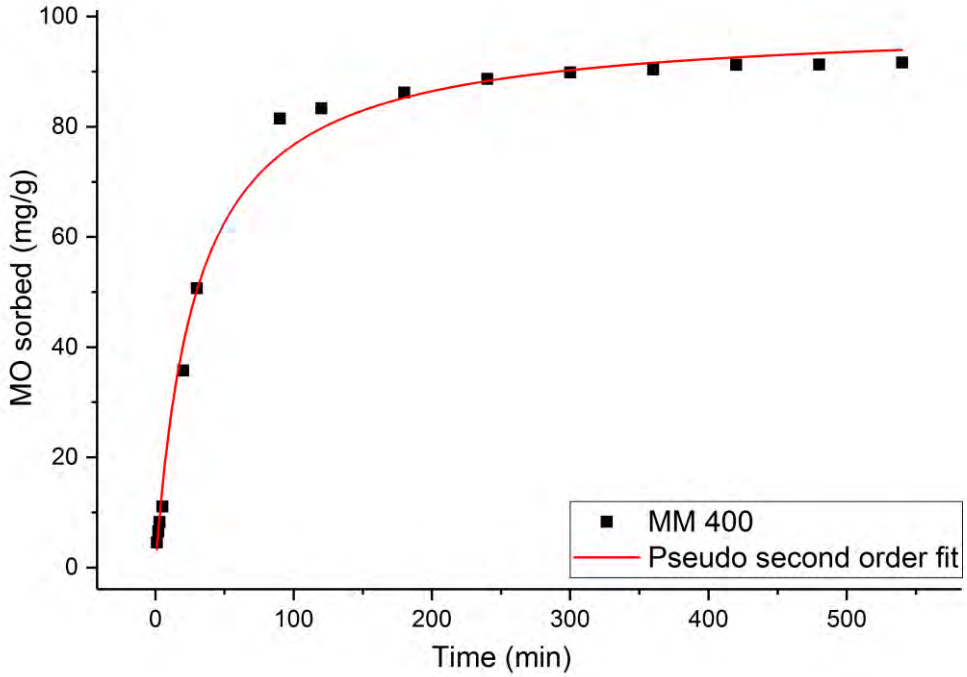

862

863 Figure 9 Pseudo-second-order fitting plot of MO adsorption onto MM 400 at room
864 temperature (25 °C)

865

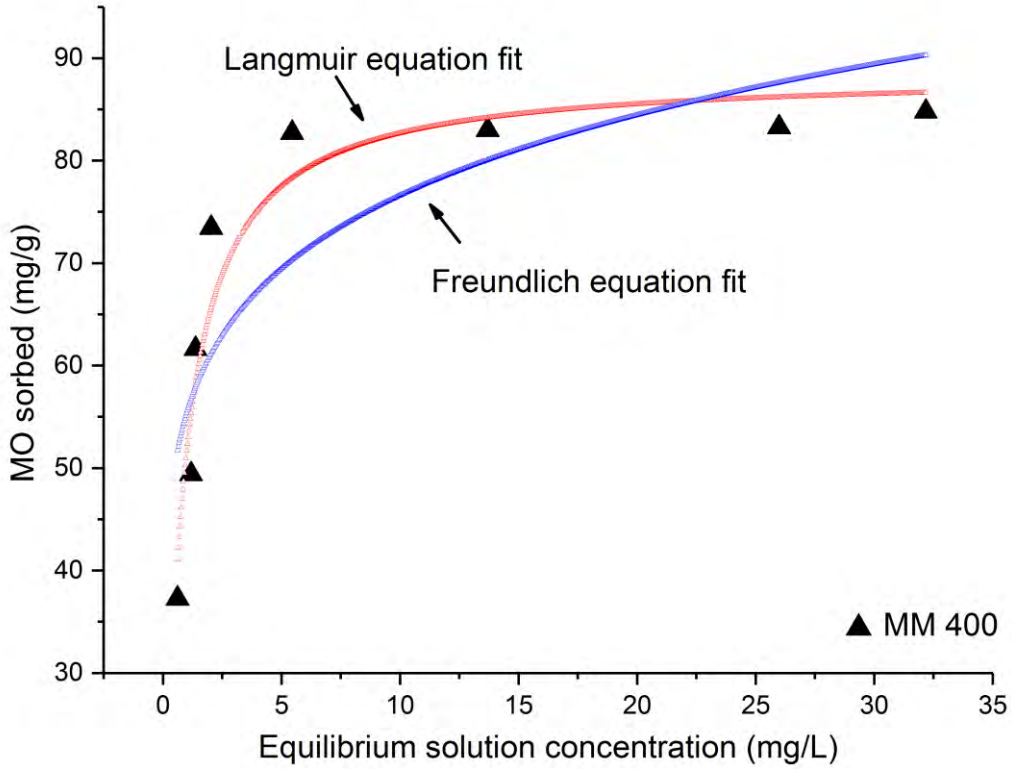

866

867 Figure 10 Langmuir and Freundlich fitting plots of MO adsorption isotherms of MM
868 400 at room temperature (25 °C)

869

This is a preprint, the final version is subject to change, of the American Mineralogist (MSA)
Cite as Authors (Year) Title. American Mineralogist, in press.
DOI: https://doi.org/10.2138/am-2020-7227

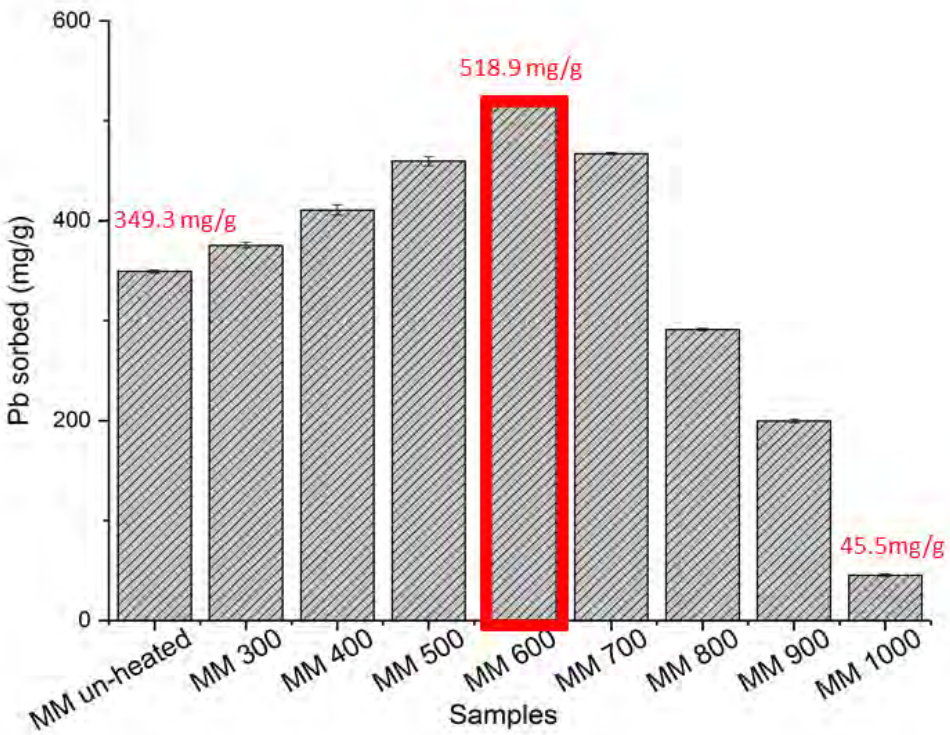

870

871 Figure 11 The maximum amounts of Pb adsorbed by MMWM samples at 25 °C
872 before (MM un-heated) and after (MM 300-1000) thermal treatment

873

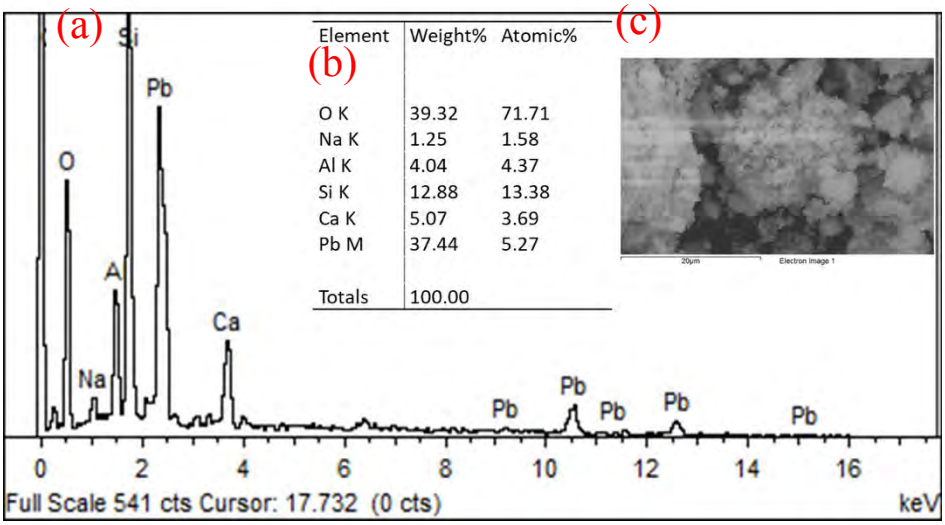

874

875 Figure 12 The EDX results of MM 600, (a) spectrum after Pb adsorption, (b)
876 element content and (c) SEM image (amplification 6.0K) used for EDX analysis.

877

This is a preprint, the final version is subject to change, of the American Mineralogist (MSA)
Cite as Authors (Year) Title. American Mineralogist, in press.
DOI: https://doi.org/10.2138/am-2020-7227

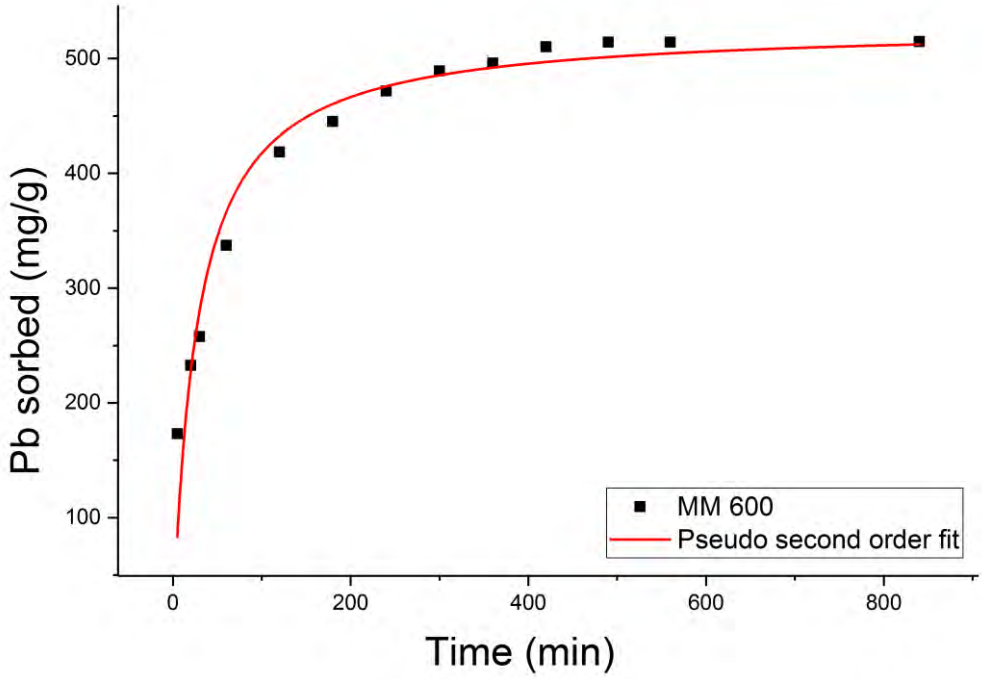

878
879 Figure 13 Pseudo-second-order fitting plot of Pb adsorption onto MM 600 at
880 room temperature (25 °C)
881

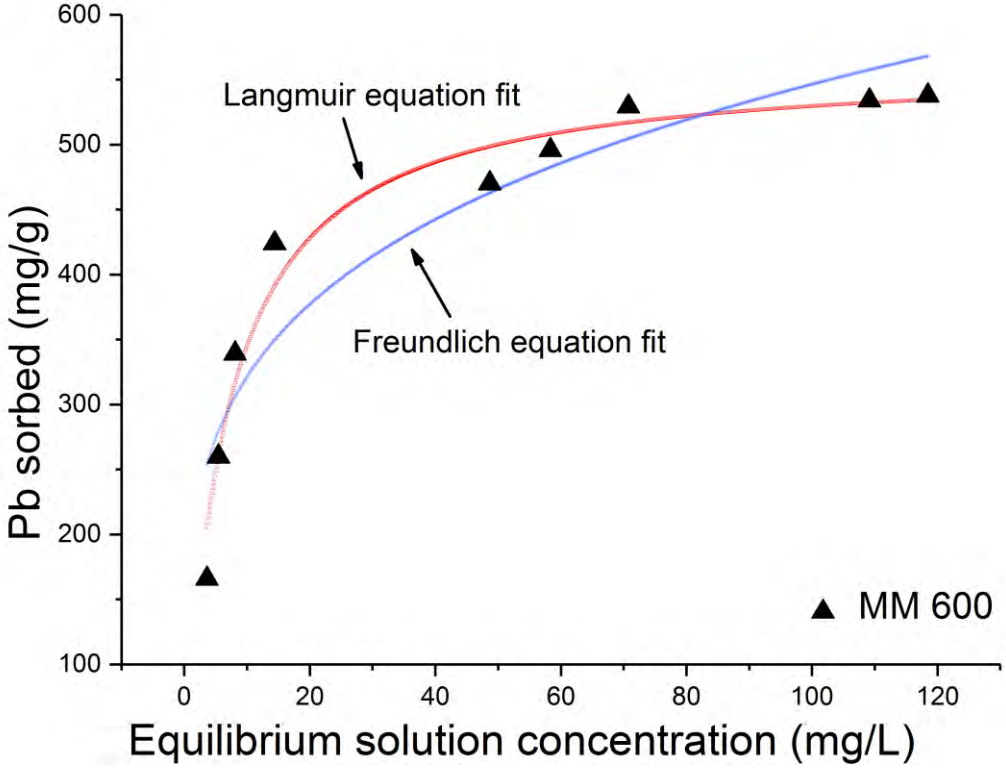

882
883 Figure 14 Langmuir and Freundlich fitting plots of Pb adsorption isotherms of
884 MM 600 at room temperature
885
886